Independent Geometrical and Electrochemical Characterization of Arrays of Nanometer-Scale Electrodes

Wendy S. Baker and Richard M. Crooks*

Department of Chemistry, Texas A&M University, P.O. Box 30012, College Station, Texas 77842-3012

Received: July 13, 1998; In Final Form: September 5, 1998

Arrays of nanometer-scale electrodes were prepared by cyanide-etching of hexadecanethiol monolayers confined to Cu-underpotential deposition (UPD)-modified Au(111). This process results in fabrication of arrays having average electrode radii ranging from 6 to 80 nm. The arrays were independently characterized by cyclic voltammetry and scanning tunneling microscopy (STM). A recessed disk model was used to calculate an expected limiting current based on the STM-derived geometrical data, and this was correlated with the electrochemically determined value. General agreement was found between these values, but nonidealities in the distribution of electrodes within the arrays led to substantial scatter in the data. We conclude that improved array characterization will result in a reliable means to test for predicted deviation from standard microelectrode theory at nanoscale electrodes. Electrochemical responses were measured for the arrays in the presence of both $Ru(NH_3)_6^{3+}$ and benzoquinone, redox probes having distinctly different heterogeneous electron-transfer rates. Highly irreversible electrochemical kinetics were observed for the kinetically slow redox probe which is a consequence of the small size of these electrodes.

Introduction

We report electrochemical and geometrical characterization of nanoelectrode arrays prepared by chemical etching of *n*-alkanethiol self-assembled monolayers (SAMs) confined to Au(111). The unique aspect of this work is that although the individual electrodes are as small as 6 nm in radius, we are able to measure their electrochemical and geometric properties *independently* using cyclic voltammetry (CV) and scanning tunneling microscopy (STM), respectively. The primary objective of this research is to probe for deviations between the theoretical and measured responses of the electrodes as their size approaches molecular dimensions. Such deviations, which have been reported previously for electrodes in this size regime,[1−3] are of fundamental importance in corrosion,[4] biological systems,[5,6] and for applications to chemical sensors.[7−9]

A common problem encountered in previous efforts to study electrodes having at least one dimension on the order of 10 nm has been a lack of information about electrode geometry. Without such information interpretation of results can be difficult or impossible.[10,11] Two studies of nanoscale electrodes have provided particularly intriguing results, however. White and co-workers fabricated band electrodes having widths ranging from 2 to 50 nm.[2,12] The thinnest of these electrodes exhibited current responses an order of magnitude smaller than predicted by standard microelectrode theory.[1,13] Additionally, significant size-related molecular recognition effects were observed as the electrode size decreased. Electrode arrays having nominal individual electrode diameters of 10 and 30 nm have been prepared by Martin et al.[14] Initial studies of these arrays yielded electrochemical responses that agreed well with theory for microelectrode arrays having overlapping diffusion regimes (linear diffusion conditions); however, the smallest electrodes exhibited an unexplained dependence on electrolyte concentration which affected both the magnitude of the peak currents as well as the reversibility of the electron transfer. Unfortunately, in neither of these studies was it possible to fully characterize the electrodes by nonelectrochemical means, so the unusual results reported in these two studies remain mysterious.

Excluding efforts to employ nanoscale electrodes as scanning electrochemical microscope (SECM) tips in single-molecule studies,[15] these two reports number among the very limited body of experimental data obtained from truly nanoscopic electrodes.[16] The paucity of information is a consequence of two factors: the challenges involved in reproducibly fabricating nanoscopic structures and then obtaining reliable topographical information. To our knowledge, this report is the first successful attempt to directly correlate independently measured geometries of nanoscopic microelectrode arrays with their electrochemical responses.

Our approach for fabricating arrays of nanoscopic electrodes is illustrated in Scheme 1. The substrate is an Au ball coated with Apiezon wax to isolate one atomically smooth Au(111) facet. The facet is modified with an underpotentially deposited Cu monolayer, which enhances the stability of SAMs and improves their resistance to thiol exchange.[17] The metal interlayer also improves the reproducibility of the etching process in comparison with unmodified Au substrates. The Cu-UPD-modified Au facet is then masked by soaking in hexadecanethiol for 24 h. Finally, the individual array elements are prepared by enlarging native defects sites within the SAM by electrochemical etching in cyanide solution.[18] Previous cyanide-etching studies of SAMs have largely focused on exploring fundamental corrosion issues,[19] or determining SAM defect densities.[20] Micron-scale electrodes have been fabricated by cyanide etching of SAMs by Yoneyhama[21] and by selective etching of short-chain alkanethiol resists anchored to micromachine-patterned Au subtrates by Whitesides.[22]

After etching, the electrochemical response of the arrays to different redox-probe molecules is measured before examining

---

* Author to whom correspondence should be addressed. Fax: (409) 845-1399. Voice: (409) 845-5629. E-mail: crooks@tamu.edu.

10.1021/jp982983g CCC: $15.00

SCHEME 1

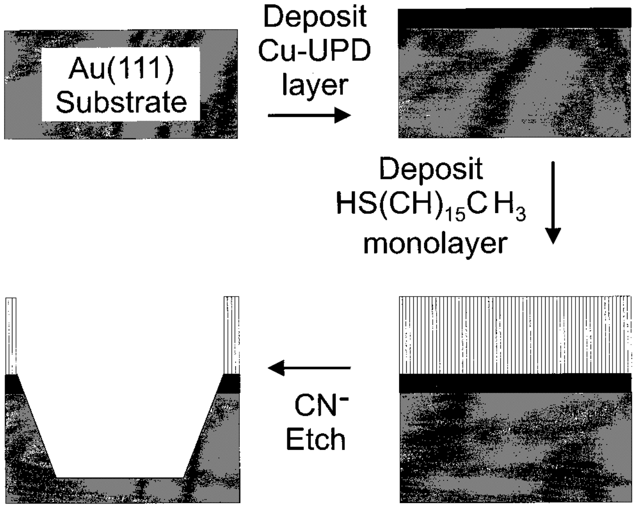

the array topology by STM. Analysis of STM images of the electrode arrays yields the average electrode radius (R_{ave}) and number density (N), parameters which can be used to calculate a "theoretical" current response. Comparison of the calculated and experimentally determined responses provides a means of quantitatively probing the behavior of nanoscopic electrode arrays. The Experimental Section provides a more detailed explanation of the array fabrication and the STM image analysis.

Experimental Section

Chemicals. The following chemicals were used as received: $HS(CH_2)_{15}CH_3$ (Fluka, 95%), KCN (Fischer, 99.9%), K_2SO_4 (Aldrich, 99%), $Na_2HPO_4 \cdot 6H_2O$ (Mallinckrodt), $Cu(ClO_4)_2 \cdot 6H_2O$ (Aldrich, 98%), 100% ethanol (Quantum), $HClO_4$ (Seastar, ultrapure), benzoquinone (Aldrich, 98%), and $Ru(NH_3)_6Cl_3$ (Strem, 99%). Deionized water (Ultrapure MilliQ water, Millipore, 18 MΩ-cm resistivity) was used to prepare aqueous solutions.

Substrate Preparation. The preparation of the Au-ball substrates has been discussed previously.[23] Briefly, substrates were prepared from Au wire (0.5 mm diameter, 99.99% purity, Refining Systems Inc., Las Vegas, NV) after cleaning in piranha solution for 10−15 min (**Caution**: Piranha, 1:3 30% H_2O_2:H_2SO_4, reacts violently with organic materials and should be immediately discarded to a waste container having a loose-fitting cap). Au balls were formed by annealing the wire in a H_2/O_2 flame. If properly annealed, the resulting balls contain several elliptically shaped Au(111) facets having typical surface areas between 3 and 6 × 10^4 μm^2. Facets are composed of atomically smooth terraces ranging from 0.5 to 1.5 μm across. The central region of a single facet was isolated by coating the remaining ball with melted Apiezon wax (Apiezon W, M&I Materials LTD, Manchester, England). This confines the electrochemical response to a single crystal face and allows well-resolved STM images to be obtained. The substrate was then placed in an ozone cleaner (Boekel UV_Clean, Model 135500, Feasterville, PA) for 10 min to remove contaminants deposited during the wax-coating process. Next, a series of cyclic voltammograms was obtained at different scan rates in 5.0 mM $Ru(NH_3)_6^{3+}$/0.1 M K_2SO_4 to determine the area of the isolated Au facet.[24] For these calculations, a diffusion coefficient of 7.1 × 10^{-6} cm^2/s was used.[25,26] It is necessary to know the area of the naked Au facet to calculate the limiting currents from the STM data, as detailed in the Results and Discussion section. Next, the facet was cleaned electrochemically by cycling between 0.1 and 1.5 V at 20 mV/s in 10 mM $Cu(ClO_4)_2$/0.1 M $HClO_4$ for 45 min and annealing for 10 min at 0.6 V. A Cu−UPD layer was deposited by removing the substrate from the cleaning solution at 0.05 V. The substrate was then rinsed with ethanol and deionized water, dried under a stream of N_2, and placed in a 1.0−1.5 mM ethanolic $HS(CH_2)_{15}CH_3$ solution for 24−28 h. After monolayer formation the substrate was rinsed again with ethanol and deionized water and then dried under flowing N_2. The next step was to ascertain the extent of substrate passivation prior to cyanide etching. This step ensures that the electrochemical response observed after etching is restricted to etched regions of the surface rather than electroactive pinholes indigenous to the monolayer. The extent to which the SAM passivated the substrate was determined by measuring the voltammetric response in a 5.0 mM $Ru(NH_3)_6^{3+}$/0.1 M K_2SO_4 electrolyte solution (scan rate: 100 mV/s). If significant Faradaic current ($>$2 nA) was observed at this stage the substrate was discarded. We then examined the substrate for passivation in 5.0 mM benzoquinone/0.1 M $HClO_4$, and applied the same criterion for electrochemical passivation.

Nanoelectrodes were introduced into the SAM by etching under potential control in 0.1 M KCN/0.1 M Na_2HPO_4. Reproducibility of array fabrication was greatly enhanced by monitoring the time-dependent current during etching. Typically, larger electrode diameters were obtained when the current response increased exponentially. Substrates were removed from the etching solution under potential control. The following etching conditions were applied to the individual substrates: Array 1, 90 s at 0.4 V; Array 2, 100 s at 0.3 V and 150 s at 0.4 V; Array 3, 100 s at 0.4 V; Array 4, 240 s at 0.2 V; Array 5, 120 s at 0.3 V and 70 s at 0.4 V and Array 6, 90 s at 0.3 V and 80 s at 0.4 V. After etching, the electrochemical response of the array was examined in 5.0 mM $Ru(NH_3)_6^{3+}$/0.1 M K_2SO_4.

Electrochemistry. A Ag/AgCl (3 M NaCl) reference electrode (Bioanalytical Systems, West Lafayette, IN), against which all potentials are reported, and a Pt gauze counter electrode were employed for all electrochemical experiments. When KCN was present in solution a small fritted glass cell filled with 0.1 M Na_2HPO_4 was employed to protect the reference electrode. Benzoquinone solutions were protected from light and deoxygenated with flowing N_2 when not in use.[27] All other solutions were air saturated. Electrochemical measurements were made with a Pine Instruments Model AFRDE4 bipotentiostat (Grove City, PA) and recorded on a Kipp and Zonen XYY′ chart recorder (Bohemia, NY).

STM Analysis. STM experiments were performed with a Digital Instruments Nanoscope III Microscope (Digital Instruments, Santa Barbara, CA). Tips were prepared from mechanically cut Pt/Ir wire (90/10, Sigmund Cohn Corp., Mount Vernon, NY). The STM D-scanner employed for these experiments was *z*-calibrated vs the theoretical Au(111) step height of 0.235 nm using a previously described procedure.[19b] Data were obtained in air using the constant-current mode with a bias voltage of 300 mV and tunneling current of 150 pA. Scan rates were typically 2−2.5 Hz. For each array, STM images were obtained from four distinct regions of the Au(111) facet. This was done to ascertain that the electrodes were evenly distributed across the surface of the facet.

Electrode areas and number densities were obtained by employing the grain-size function of the microscope software, under reverse thresholding conditions (NanoScope Software Version 4.23). Surface depressions at least three Au atomic step heights ∼(0.7 nm) deeper than the surrounding Au terrace

TABLE 1: Geometrical Characteristics of Individual Electrodes and Experimental and Calculated Limiting Currents for Electrode Arrays

array number	facet area (A) (10^3 μm^2)	average electrode radius (R_{ave}) (nm)[a]	average electrode depth (nm)[b]	electrode number density (electrodes/μm^2)[a]	average center-to-center electrode separation (μm)[c]	average diffusion-layer thickness (μm)[d]	i_{lim} exptl (nA)[c]	i_{lim} STM inlaid disk (nA)[f]	i_{lim} STM recessed disk (nA)[g]	i_{lim} STM recessed disk/i_{lim} exptl
1	11.1	50	5	0.6	1.3	0.3	100	430	410	4
2	16.0	7	2	0.1	3.2	0.04	40	15	11	0.3
3	16.3	80	25	0.3	1.8	0.5	180	550	530	3
4	22.3	10	2	0.5	1.4	0.06	20	150	120	6
5	17.2	9	3	0.5	1.4	0.05	16	110	80	5
6	12.4	6	2	0.2	2.2	0.04	13	19	13	1

[a] Average electrode radii and electrode number density data were determined from STM data obtained on four different regions of the same Au(111) facet. 500 nm × 500 nm and 1 μm × 1 μm STM images totaling 10 μm^2 were employed for the analysis. The electrode area was determined at a threshold depth equivalent to 3 Au atomic step heights below the surrounding Au terrace. [b] The average electrode depth is the average distance between the Au terrace and the most recessed region of the electrode. [c] The average electrode separation value assumes that the electrodes reside at regular intervals along a square grid with an electrode number density identical to the STM-determined value. [d] The average diffusion-layer thickness is 6R_{ave}. [e] Cyclic voltammetry was performed in aqueous 5.0 mM $Ru(NH_3)_6^{3+}$/0.1 M K_2SO_4, scan rate: 100 mV/s. [f] Calculated from STM data and eq 1. [g] Calculated from STM data and eq 2.

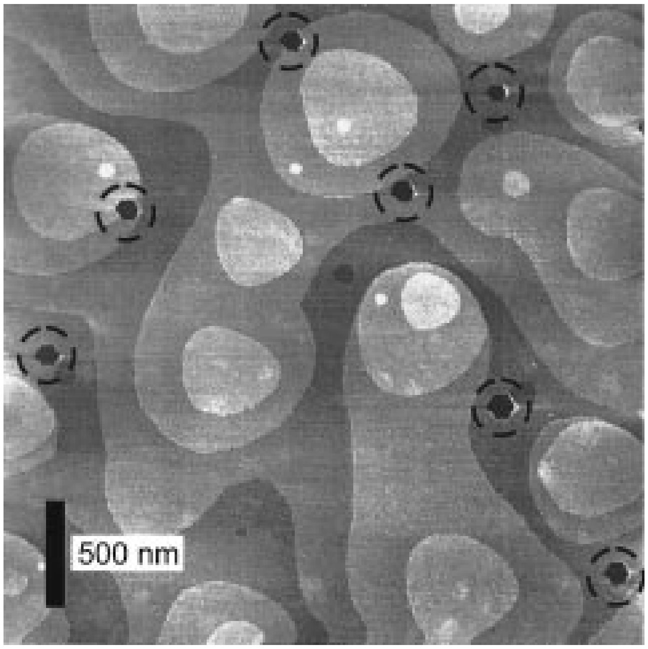

Figure 1. A 3 μm × 3 μm STM image obtained from Array 1 (Table 1). The seven individual microelectrodes in this image are highlighted; other features apparent in the image are Au terraces.

were included in the electrode count. Surface pitting of this depth is absent on unetched samples and is easily distinguished from native electroinactive thiol pits.[28] The electrode radii were calculated by fitting the area of each recessed region to a disk-shaped model of equivalent area. The section analysis function was used to determine electrode depths, which were measured from the most recessed regions of the pits to minimize the effects of tip morphology on the depth measurements. The average center-to-center electrode separation for each array (Table 1) was calculated by assuming the electrodes to be evenly distributed across a square grid having the STM-determined electrode density.

Results and Discussion

Figure 1 is an STM image representing a small fraction of the surface of Array 1 (Table 1). In this image, seven electrodes of highly consistent geometry are apparent. The hexagonal shape of the individual electrodes is a consequence of the underlying symmetry of the Au(111) surface.[19b,c] The measured, average electrode radius for this array is 50 nm, a value calculated by fitting the STM-determined areas to a disk-shaped electrode model. The measured electrode number density is 0.6 electrodes/μm^2, the highest of the six arrays examined, and the average separation between the electrodes is 1.3 μm. Previous work has shown that the steady-state diffusion layer thickness for an individual nanoelectrode will extend approximately 6R_{ave} (R_{ave} is the average electrode radius) outward from the center of each electrode.[29,30] For Array 1 this value is 0.3 μm, thus the electrode separation required to avoid shielding of nearest-neighbor electrodes is 0.6 μm. Because the average electrode separation (1.3 μm) exceeds twice the average diffusion-layer thickness (0.6 μm), there should be no overlap of the diffusion layers of the individual electrodes. Since Array 1 represents the worst-case scenario, there should be no overlap for any of the other arrays described in Table 1, and thus the current response from each array should be a simple sum of the current response from each electrode.

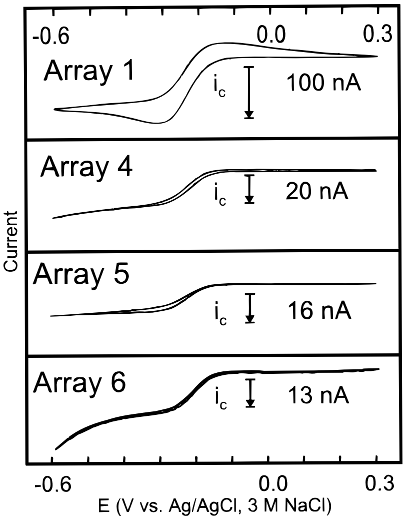

Figure 2. Cyclic voltammetric response for Arrays 1,4–6 obtained after cyanide etching. The voltammetric response was negligible for all electrodes prior to etching. Voltammograms were obtained in 5.0 mM $Ru(NH_3)_6^{3+}$/0.1 M K_2SO_4, scan rate: 100 mV/s. The voltammetry for arrays 2 and 3 is shown in Figure 3.

In contrast to the STM data, the nonideal voltammetry obtained for $Ru(NH_3)_6^{3+}$ at Array 1 (Figure 2) suggests that some overlap of the individual diffusion layers does occur. This is apparent from the shape of the CV: non-steady-state current and a significant hysteresis between the forward and backward scans. This observation serves to point out a significant limitation of our array fabrication method; currently it is not possible to control electrode placement, and therefore the distribution of individual electrodes is nonuniform. Thus, although the average spacing between electrodes is greater than the steady-state diffusion layer thickness, there is overlap for certain pairs of electrodes leading to nonideal voltammetric behavior. At present, the only way to avoid this problem is to prepare arrays with very low electrode densities so the likelihood of cross-talk between electrodes is minimized.

Figure 3 shows STM and electrochemical data for typical etching experiments. An STM image obtained from Array 2 (Figure 3, part a) reveals a 10 nm-radius electrode having a depth of approximately 2 nm. Prior to etching, the substrate is very well passivated by the SAM layer (Figure 3, part b), but afterward nearly ideal steady-state voltammetry is obtained, yielding a limiting current of 40 nA from a solution containing 5.0 mM $Ru(NH_3)_6^{3+}$/0.1 M K_2SO_4 (Figure 3, part c). The STM-determined average electrode density (Table 1) is 0.1 electrode/μm^2, and the calculated average electrode separation is 3.2 μm. Based on the average electrode radius (7 nm) the diffusion layer thickness is only 0.04 μm, almost 2 orders of magnitude smaller than the average electrode separation. Thus, for this array it is reasonable to expect that radial diffusion will dominate the voltammetric response as is indicated by the data.

The other STM image in Figure 3 was obtained from Array 3. This image shows a single hexagonal electrode approximately 100 nm in radius. The voltammetry reveals passivation prior to etching and a large current increase after etching; the limiting current is about 180 nA. The voltammetric response exhibits characteristics of both radial and linear diffusion.[29] Based on the magnitude of the diffusion layer thickness (0.5 μm) relative to the average electrode separation (1.8 μm) this behavior is reasonable in light of the aforementioned imperfections in the electrode distribution.

Table 1 provides detailed information about the three arrays already described as well as data obtained from three additional arrays. The table indicates that nanoscopic microelectrode arrays of a variety of different geometries can be prepared using the described fabrication procedure. The average electrode radii for the six arrays range between 6 and 80 nm, while the number densities vary between 0.1 and 0.6 electrodes/μm^2. Average electrode depths range from 2 to 25 nm. The geometrical similarities of Arrays 4 and 5 and Arrays 2 and 6 show that a measure of reproducibility is allowed by the electrode fabrication technique. On the basis of the STM-derived geometrical data, calculated limiting currents can be determined for two different model systems: inlaid- and recessed-disk electrodes. The relationships between limiting currents (i_{lim}) and the average electrode radius (R_{ave}) and number density (N) for these two geometries are given in eq 1 and eq 2, respectively.[30,31]

$$i_{\mathrm{lim}} = 4nFR_{\mathrm{ave}}CDNA \tag{1}$$

$$i_{\mathrm{lim}} = \frac{4\pi nFR_{\mathrm{ave}}^{2}CDNA}{4L + \pi R_{\mathrm{ave}}} \tag{2}$$

The variables F, C, D, A, and n are, respectively, the Faraday, the redox-probe concentration, the redox-probe diffusion coefficient, the area of the naked Au facet, and the equivalents of electrons transferred per mole of redox molecule. In performing the calculations for the recessed-disk model, the height of the insulating layer (L) was assumed to be 2.1 nm—the $CH_3(CH_2)_{15}$-SH monolayer thickness.

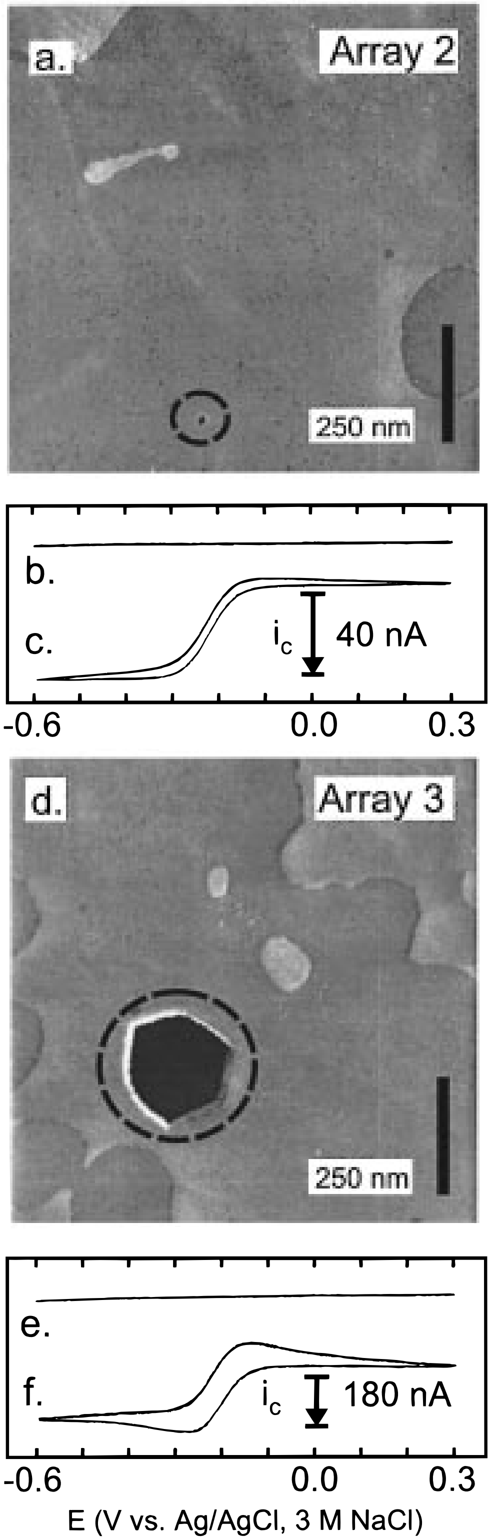

Figure 3. (a) 1 μm × 1 μm STM image of Array 2 (Table 1). A 10 nm-radius microelectrode is highlighted. (b) Cyclic voltammogram obtained from Array 2 before etching. (c) Cyclic voltammogram obtained from Array 2 after etching. (d) 1 μm × 1 μm STM image of Array 3. A 100 nm-radius hexagonal-shaped microelectrode is highlighted. (e) Cyclic voltammogram obtained from Array 3 before etching. (f) Cyclic voltammogram obtained from Array 3 after etching. All voltammograms were obtained in 5.0 mM $Ru(NH_3)_6^{3+}$/0.1 M K_2SO_4; scan rate: 100 mV/s.

The experimentally measured limiting current response was most closely approximated by the recessed-disk electrode model for five of the six arrays (Table 1). Using this model, we found that the ratio of the calculated to electrochemically determined limiting currents ranges from 6 to 0.3. We believe the

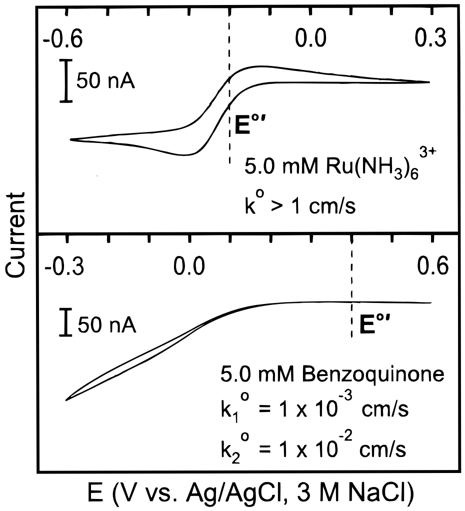

Figure 4. Cyclic voltammetric response for Array 1 in 5.0 mM Ru$(NH_3)_6{}^{3+}$/0.1 M K_2SO_4 and 5.0 mM benzoquinone/0.1 M $HClO_4$; scan rate: 100 mV/s.

calculated currents deviate from the experimental values for three principal reasons. First, irregularities in the electrode distribution result in diffusional shielding among individual electrodes. For example, in Figures 2 and 3 the voltammograms from Arrays 1 and 3 exhibit effects attributable to linear diffusion. This observation is consistent with the data in Table 1, which indicate that the calculated average diffusion layer thicknesses for the individual electrodes in these arrays approach the average electrode separation distances.

Second, the inlaid- and recessed-disk models are imprecise approximations of the actual electrode geometries. A more adequate model would describe the flux of electroactive species into the internal cavity of a recessed cylindrical well having an electroactive wall and base (Scheme 1), but to the best of our knowledge the flux equations for this electrode geometry have not been solved. Additionally, neither of the models used here incorporates possible effects resulting from the nonrigid, hydrophobic monolayer insulator. The recessed-disk model, for example, assumes that the insulating layer is rigid and oriented normal to the surface. An insulating thiol monolayer, however, may become disorganized around the edge of the electrode and act to block the flux of electroactive species into the electrode. The magnitude of this effect would necessarily increase as the size of the electrodes decreases. This factor may help explain the relatively large deviation between the calculated and electrochemically determined responses of Arrays 4 and 5.

Finally, the nature of our STM sampling method may introduce a bias into the calculated values of the limiting currents. Multiple STM images (composed of 500 nm × 500 nm and 1 μm × 1 μm scans) were obtained from four different regions of each facet. Image analysis was performed on 10 μm^2 of the electrode by examining an appropriate number of these images in randomly chosen combinations. Since a relatively small surface area was employed in the image analysis (typically 0.05% of the total surface), the presence of unusually small or large electrodes (outliers) in one of the analyzed images will significantly affect the STM-measured average electrode radius and number density. In the future we plan to reduce the effect of this problem by increasing the fractional area of the surface analyzed.

Figure 4 shows the electrochemical behavior of Array 1 in 5.0 mM $Ru(NH_3)_6{}^{3+}$/0.1 M K_2SO_4 and 5.0 mM benzoquinone/0.1 M $HClO_4$. In $Ru(NH_3)_6{}^{3+}$, the half-wave potential ($E_{1/2}$) occurs very close to the formal electrode potential of the redox probe. This behavior is reasonable in light of the fast rate of electron transfer of $Ru(NH_3)_6{}^{3+}$ (>1 cm/s).[32] The benzoquinone voltammetry is highly irreversible: $E_{1/2}$ is shifted more than 200 mV negative of the formal electrode potential of 0.4 V.[33] This result is consistent with the slow, rate-limiting electron transfer step for benzoquinone (1×10^{-3} cm/s) compared to the fast electron transfer of $Ru(NH_3)_6{}^{3+}$.[32,34] The potential shift in $E_{1/2}$ for benzoquinone is in agreement with predicted behavior for slow apparent electron transfer processes at blocked surfaces containing a small number of widely separated electrodes.[35,36] A more thorough examination of this phenomenon will be presented in a future publication.

Conclusions

We have shown that cyanide etching of *n*-alkanethiol monolayers bound to Cu−UPD-modified Au(111) provides a reliable method for fabrication of nanoelectrode arrays. A unique advantage of these arrays is that they may be characterized independently by both electrochemistry and scanning probe microscopy. The experimental limiting current responses for $Ru(NH_3)_6{}^{3+}$ were on average a factor of 3 smaller than the limiting currents calculated for the recessed-disk electrode model using the STM-derived parameters (average electrode radius and number densities). This apparent deviation between experiment and theory may be a limitation of the fabrication and analysis methods rather than a result of an unexpected physical phenomenon. Possible reasons for the deviation include diffusional shielding among unevenly distributed electrodes, discrepancies between the true electrode geometry and the geometry inherent to the model, blocking of the electrode by the flexible monolayer, and the small fractional sampling of the array surface area used in the STM analysis. In future studies we plan to examine ways to minimize these effects: first, by increasing the surface area employed for STM analysis and then by exploring means to improve the electrode distributions and geometrical consistency. We believe these refinements will allow us to accurately probe the validity of standard microelectrode theories for very small electrodes. Finally, in the presence of a redox probe having a slow standard electron transfer rate, we observed shifts in the value of $E_{1/2}$ in agreement with predicted behavior for small, widely separated electrodes. This observation is consistent with our STM-derived geometrical data.

Acknowledgment. We acknowledge the National Science Foundation (CHE-9313441) for financial support of this work. Valuable discussions with Professor Allen J. Bard (University of Texas), Dr. Stephen W. Feldberg (Brookhaven National Laboratory), Professor Henry S. White (University of Utah), and Professor Cynthia G. Zoski (University of Rhode Island) are also gratefully acknowledged.

References and Notes

(1) Wehmeyer, K. R.; Deakin, M. R.; Wightman, R. M. *Anal. Chem.* **1985**, *57*, 1913.

(2) Morris, R. B.; Franta, D. J.; White, H. S. *J. Phys. Chem.* **1987**, *91*, 3559.

(3) Michael, A. C.; Wightman, R. M. "Microelectrodes" In *Laboratory Techniques in Electroanalytical Chemistry*, 2nd ed.; Kissinger, P. T., Heineman, W. R., Eds.; Marcel Dekker: New York, 1996; pp 367−399.

(4) (a) Turnbull, A. Mathematical Modelling of Localized Corrosion. In *Modelling Aqueous Corrosion*; Trethewey, K. R., Roberge, P. R., Eds.; NATO ASI Series E, Vol. 266; Kluwer: Boston, 1994; pp 29−63. (b) Trethewey, K. R.; Sargeant, D. A.; Marsh, D. J.; Haines, S. New Methods of Quantitative Analysis of Localized Corrosion Using Scanning Electrochemical Probes. In *Modelling Aqueous Corrosion*; Trethewey, K. R.,

Roberge, P. R., Eds.; NATO ASI Series E, Vol. 266; Kluwer: Boston, 1994; pp 417−442.

(5) Chen, T. K.; Luo, G.; Ewing, A. G. *Anal. Chem.* **1994**, *66*, 3031.

(6) Kawagoe, K. T.; Jankowski, J. A.; Wightman, R. M. *Anal. Chem.* **1991**, *63*, 1589.

(7) Janata, J. *Principles of Chemical Sensors*; Plenum: New York, 1989; pp 181−186.

(8) Janata, J. *Chem. Rev.* **1990**, *90*, 691.

(9) Abruña, H. D.; Pariente, F.; Alonso, J. L.; Lorenzo, E.; Trible, K.; Cha, S. K. Electroanalytical Strategies with Chemically Modified Interfaces. In *Interfacial Design and Chemical Sensing*; Mallouk, T. E., Harrison, D. J., Eds.; ACS Symposium Series 561; American Chemical Society: Washington, D. C., 1994; pp 230−243.

(10) Penner, R. M.; Heben, M. J.; Longin, T. L.; Lewis, N. S. *Science* **1990**, *250*, 1118.

(11) Oldham, K. B. *Anal. Chem.* **1992**, *64*, 646.

(12) Seibold, J. D.; Scott, E. R.; White, H. S. *J. Electroanal. Chem.* **1989**, *264*, 281.

(13) (a) Jeager, J. C. *Proc. R. Soc. Edinburgh* **1942**, *A61*, 223. (b) Kovach, P. M.; Caudill, W. L.; Peters, D. G.; Wightman, R. M. *J. Electroanal Chem.* **1985**, *185*, 285.

(14) (a) Menon, V. P.; Martin, C. R. *Anal. Chem.* **1995**, *67*, 1920. (b) Ugo, P.; Moretto, L. M.; Bellomi, S.; Menon, V. P.; Martin, C. R. *Anal. Chem.* **1996**, *68*, 4160. (c) Martin, C. R. *Science* **1994**, *266*, 1961. (d) Cepak, V. M.; Hulteen, J. C.; Che, G.; Jirage, K. B.; Lakshmi, B. B.; Fisher, E. R.; Martin, C. R.; Yoneyhama, H. *Chem. Mater.* **1997**, *9*, 1065.

(15) (a) Bard, A. J.; Fan, F.-R. *Acc. Chem. Res.* **1996**, *29*, 572. (b) Fan, F.-R.; Kwak, J.; Bard, A. J. *J. Am. Chem. Soc.* **1996**, *118*, 9669. (c) Lee, C.; Miller, C. J.; Bard, A. J. *Anal. Chem.* **1991**, *63*, 78. (d) Mirkin, M. V.; Fan, F.-R.; Bard, A. J. *J. Electroanal. Chem.* **1992**, *328*, 47. (e) Fan, F.-R.; Bard, A. J. *Science* **1995**, *267*, 871.

(16) (a) Hulteen, J. C.; Menon, V. P.; Martin, C. R. *J. Chem. Soc., Faraday Trans. 1* **1996**, *92*, 4029. (b) Padeste, C.; Kossek, S.; Lehmann, H. W.; Musil, C. R.; Gobrecht, J.; Tiefenauer, L. *J. Electrochem. Soc.* **1996**, *143*, 3890.

(17) (a) Jennings, G. K.; Laibinis, P. E. *Langmuir* **1996**, *12*, 6173. (b) Jennings, G. K.; Laibinis, P. E. *J. Am. Chem. Soc.* **1997**, *119*, 5208. (c) Zamborini, F. P.; Campbell, J. K.; Crooks, R. M. *Langmuir* **1998**, *14*, 640.

(18) (a) Kirk, D. W.; Foulkes, F. R.; Graydon, W. F. *J. Electrochem. Soc.* **1978**, *125*, 1436. (b) Kirk, D. W.; Foulkes, F. R. *J. Electrochem. Soc.* **1980**, *127*, 1993. (c) Zamborini, F. P.; Crooks, R. M. *Langmuir* **1997**, *13*, 122.

(19) (a) McCarley, R. L.; Bard, A. J. *J. Phys. Chem.* **1992**, *96*, 7410. (b) Sun, L.; Crooks, R. M. *Langmuir* **1993**, *9*, 1951. (c) Zamborini, F. P.; Crooks, R. M. *Langmuir* **1998**, *14*, 3279.

(20) (a) Chailapakul, O.; Sun, L.; Xu, C.; Crooks, R. M. *J. Am. Chem. Soc.* **1993**, *115*, 12459. (b) Zhao, X. M.; Wilbur, J. L.; Whitesides, G. M. *Langmuir* **1996**, *12*, 3257.

(21) Ohtani, M.; Sunagawa, T.; Kuwabata, S.; Yoneyhama, H. *J. Electroanal. Chem.* **1997**, *429*, 75.

(22) Abbott, N. L.; Rolison, D. R.; Whitesides, G. M. *Langmuir* **1994**, *10*, 2672.

(23) (a) Hsu, T.; Cowley, J. M. *Ultramicroscopy* **1983**, *11*, 239. (b) Snyder, S. R. *J. Electrochem. Soc.* **1992**, *139*, 5C. (c) Sun, L.; Crooks, R. M. *J. Electrochem. Soc.* **1991**, *138*, L23.

(24) The equation for the area calculation is $i_p = (2.69 \times 10^5)\ n^{3/2}\ A\ D^{1/2}\ v^{1/2}\ C$ where i_p is the peak current of a linear sweep voltammogram (A), n is the number of electrons transferred, A is the electrode area (cm^2), D is the diffusion coefficient (cm^2/s), v is the scan rate (V/s), and C is concentration (mol/cm^3). Bard, A. J.; Faulkner, L. R. *Electrochemical Methods*; John Wiley: New York, 1980; Chapter 6.

(25) Bard, A. J.; Crayston, J. A.; Kittlesen, G. P.; Shea, T. V.; Wrighton, M. S. *Anal. Chem.* **1986**, *58*, 2321.

(26) Licht, S.; Cammarata, V.; Wrighton, M. S. *J. Phys. Chem.* **1990**, *94*, 6133.

(27) Chambers, J. Q. Electrochemistry of Quinones. In *The Chemistry of the Quinonoid Compounds*; Patai, S., Rappoport, Z., Eds.; Chemistry of Functional Groups, Vol. 2, Pt. 1; Wiley: New York, 1988; pp 719−757.

(28) Ross, C. B.; Sun, L.; Crooks, R. M. *Langmuir* **1993**, *9*, 632.

(29) Wightman, R. M.; Wipf, D. O. Voltammetry at Ultramicroelectrodes. In *Electroanalytical Chemistry*, Vol. 15; Bard, A. J., Ed.; Dekker: New York, 1989; pp 267−353.

(30) Saito, Y. *Rev. Polarogr.* **1968**, *15*, 177.

(31) Bond, A. M.; Luscombe, D.; Oldham, K. B.; Zoski, C. G. *J. Electroanal. Chem.* **1988**, *249*, 1.

(32) Endicott, J. F.; Schroeder, R. R.; Chidester, D. H.; Ferrier, D. R. *J. Phys. Chem.* **1973**, *77*, 2579.

(33) The standard electrode potential was obtained experimentally in 5.0 mM benzoquinone/0.1 M HClO$_4$ at a Au-wire working electrode.

(34) Laviron, E. *J. Electroanal. Chem.* **1984**, *164*, 213.

(35) Amatore, C.; Savéant, J. M.; Tessier, D. *J. Electroanal. Chem.* **1983**, *147*, 39.

(36) Bond, A. M.; Oldham, K. B.; Zoski, C. G. *Anal. Chim. Acta* **1989**, *216*, 177.